Supplementary Information

ENGINEERED MESOPOROUS SILICA-BASED NANOPARTICLES AS SMART CHEMOTHERAPY FOR BORTEZOMIB ADMINISTRATION

M. De Santo[a], A. Giovinazzo[b], M. Fava[a], E. Mazzotta[c], I. E. De Napoli[b], M. Greco[a], A. Comandé[a], A. Nigro[a], P. Argurio[b], I. Perrotta[d], M. Davoli[d], A. Tagarelli[e], R. Elliani[e], G. Nicolini[c], A. Chiorazzi[c], S. Semperboni[c], E. Ballarini[c], C. Crocamo[c], G. Cavaletti[c], D. Lombardo[f], D. Sisci[a], C. Morelli [a‡], A. Leggio [a‡*], L. Pasqua [b‡*]

[a] Department of Pharmacy, Health and Nutritional Sciences, University of Calabria, via P. Bucci, 87036 Arcavacata di Rende (CS), Italy;
[b] Department of Environmental Engineering University of Calabria, via P. Bucci, 87036, Arcavacata di Rende (CS), Italy;
[c] Experimental Neurology Unit, School of Medicine and Surgery and Milan Center for Neuroscience, University of Milano-Bicocca, via Cadore 48, 20900 Monza, Italy;
[d] Department of Biology, Ecology and Earth Sciences, Centre for Microscopy and Microanalysis (CM2), Transmission Electron Microscopy Laboratory, University of Calabria, via P. Bucci, 87036 Arcavacata di Rende (CS), Italy;
[e] Department of Chemistry and Chemical Technologies, University of Calabria, via P. Bucci, 87036 Arcavacata di Rende (CS), Italy;
[f] Institute for Chemical-Physical Processes, National Research Council, 98158 Messina, Italy.
‡equally share the last authorship
* Corresponding authors

* *Contact Information*: Luigi Pasqua
Department of Environmental Engineering,
Via P. Bucci, cubo 44/a
University of Calabria, 87036 Arcavacata di Rende (CS) Italy;
Tel: +39 0984 496642, FAX: +39 0984 496651
E-mail: l.pasqua@unical.it

Supplementary Text

Among the various existing silica nanoparticles to be used in Drug Delivery Systems (DDS), MSNs remain the safest choice.[1]

This might stem from the observation that MSNs are degraded into smaller oligomers and water-soluble orthosilicic acid $Si(OH)_4$ which are easily excreted by urines. In addition, shape, surface features, and pore size seem to greatly affect MSNs biocompatibility and biodistribution.[2]

Folate receptors (FRs) have been widely recognized as interesting Tumor Associated Antigens (TAAs) since high levels of FRs are expressed by several types of cancers, compared to lower or no expression in normal cells.[3] Of the four known human isoforms (α, β, γ, and δ), each with tissue-specific distribution, [4] the membrane glycosylphosphatidylinositol (GPI)-anchored α and β isoforms have been reported to internalize

folates and folate conjugated compounds via receptor-mediated endocytosis.[5] Therefore, being particularly important for highly proliferating cancer cells, folic acid has been widespread recognized as a targeting function that could be anchored on MSNs external surface and exploited to target imaging molecules and therapeutic compounds directly to cancerous tissues.[6]

Multiple Myeloma (MM) is a B-cell malignancy characterized by abnormal proliferation of plasma cells that secrete monoclonal immunoglobulins and accounts for 15% of hematopoietic cancers. Proteasome inhibitors are the main therapeutic choice for this malignancy, causing a high accumulation of misfolded or unfolded proteins in the endoplasmic reticulum (ER) of MM cells, activating, in turn, apoptotic pathways and, consequently, leading cells to death.[7]

Bortezomib (BTZ), a dipeptide boronic acid, is a synthetic compound belonging to a class of antineoplastic agents which act by inhibiting the chymotrypsin-like activity of proteasome 26S.[8,9] It is the first-in-class proteasome inhibitor approved by US FDA for the treatment of MM patients.

Supplementary Results and Discussion

Synthesis of the starting MSNs

Mesoporous silica nanoparticles used in this study were synthesized by modifying an interfacial synthesis procedure carried out at room temperature, using cyclohexane as the organic upper phase, in which the silica source, tetraethyl orthosilicate (TEOS), is dissolved. Surfactant micelles from the lower water phase encounter the silica source in the interfacial region, where silica polymerization occurs. No mineralizing agents are used for this synthesis procedure, carried out at neutral pH (comprised between 8 and 7). If compared to the original MSU synthesis[10] lower surfactant/water ratio are employed and higher cell parameter and pore size are obtained. A defective amorphous mesoporous silica framework rich in hydroxyl groups (very likely able to be degraded by hydrolysis in smaller oligomers in the medium term) with thick pore walls is obtained. Furthermore, the uncontrolled growth of the particles is avoided because the synthesis, as above reported, occurs in the interfacial region and larger particles sediments towards the bottom of the synthesis vessel where silica is no more feed and their growth is no more possible. This was aimed to limit mesoporous silica particle size, an essential parameter in drug targeting applications.

Solid-State NMR analysis of FOL-MSN-BTZ

FOL-MSN-BTZ was characterized using ^{29}Si and ^{13}C solid state NMR. In ^{29}Si NMR spectrum two intense peaks at around -110 and -101 ppm corresponding to the structures $Q^4[Si(OSi)_4]$ and $Q^3[Si(OSi)_3OH]$ are observed. The presence of signals at around -66 and -57 ppm from $T^3[RSi(OSi)_3]$ and $T^2[RSi(OSi)_2OH]$ silicon sites **(Figure S1a)** respectively confirm the covalent bonding of silica framework with organosilanes. Solid-state ^{13}C NMR spectrum **(Figure S1b)** shows signals associated to both the organic ligands and bortezomib molecule. The signal corresponding to the carbons of the silicon-bound methylene groups (Si-CH_2) appears at around 10 ppm while the other signals in the aliphatic region (23-56 ppm) can be associated to the methylene carbon atoms of the linkers and to the methyl (CH_3), methylene (-CH_2) and methine (-CH) carbon atoms of BTZ and FOL. Instead, the signals in the range 67-73 ppm are related to the carbon atoms of -OCH2, and –OCH groups of the diol linker and the cyclic boronate ester. In this same range (67-73 ppm) of the spectrum fall the resonances corresponding to carbon atoms of surfactant residues (Triton X-100). In the range 123-150 ppm the spectrum shows overlapping contributions related to the aromatic carbons of bortezomib and folic acid molecules. In addition, at around 163 ppm, it is possible to observe the presence of a broad and low intensity peak that can be assigned to the amide carbonyls of bortezomib and folic acid. The presence in the spectrum of relatively broad peaks is indicative of a solid type behavior.

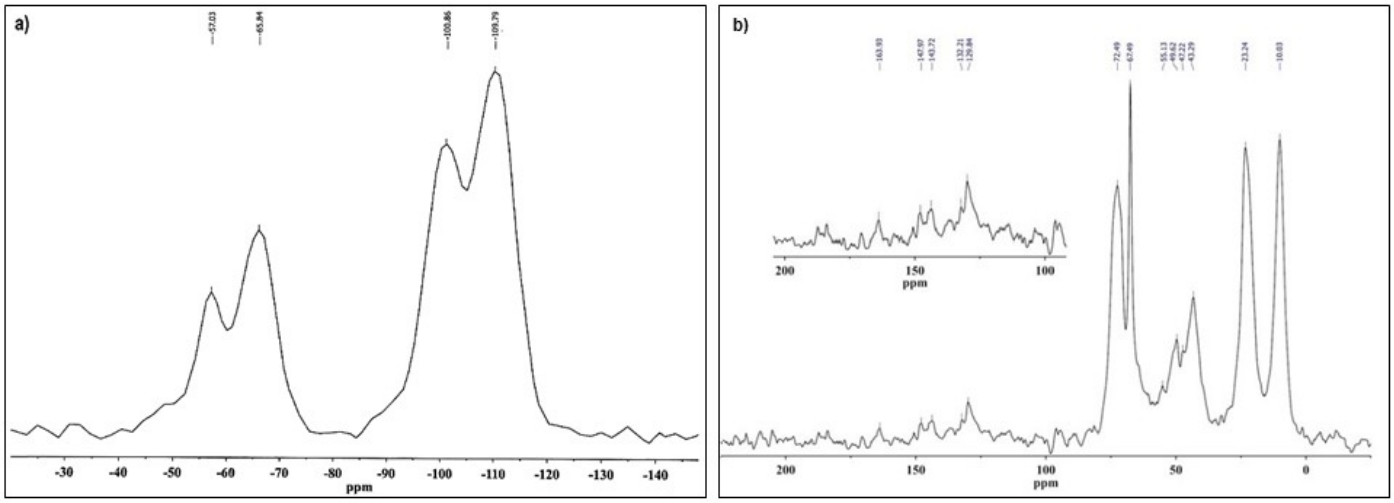

Figure S1. Solid-state ^{29}Si NMR (**a**) and ^{13}C NMR (**b**) spectra of FOL-MSN-BTZ.

Energy Dispersive X-ray analysis

Quantitative evaluation of silicon (Si) and boron (B) compositions in analysed samples by Energy Dispersive X-ray analysis (EDAX) carried out on the surface of LF, MF, and HF samples are shown in **Table S1**.

Sample	B (wt %)	**B/Si**	Si (wt %)
LF-MSN-BTZ	0.070	**0.0271**	2.58
MF-MSN-BTZ	0.101	**0.0047**	21.40
HF-MSN-BTZ	0.073	**0.0025**	29.10

Table S1. Quantitative evaluation of Si and B compositions in analyzed samples.

Polychromatic elemental maps (**Figures S2, S3, and S4**) show a high quantitative sensitivity in reference to the spatial distribution of silicon and boron on the sample surfaces.

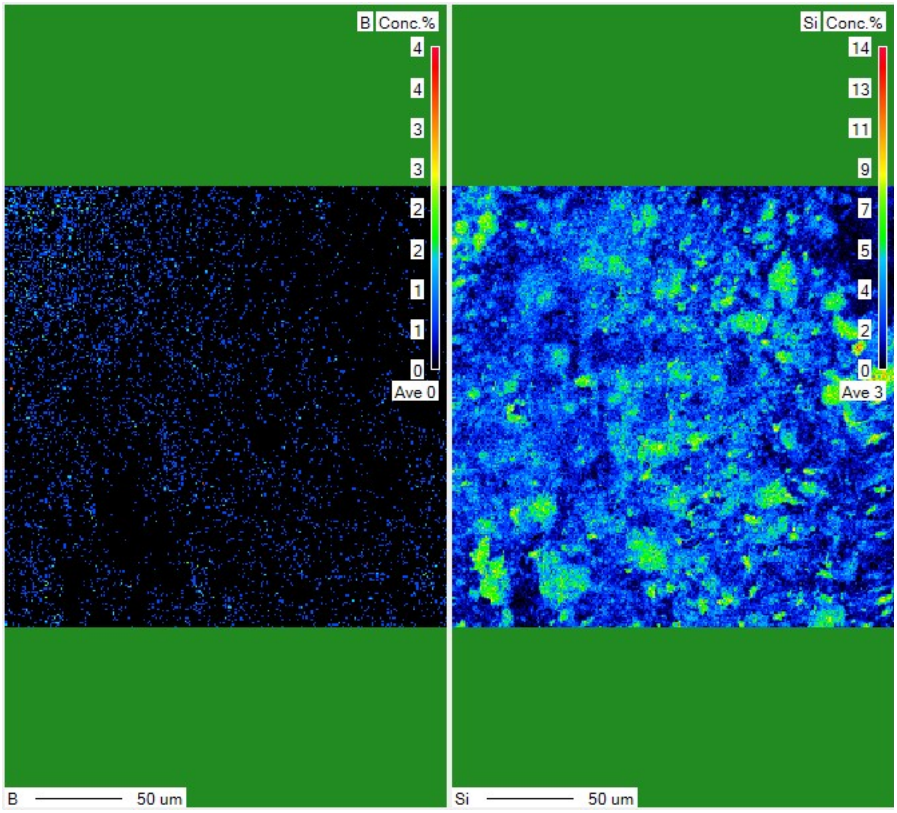

Figure S2. Polychromatic elemental maps for sample LF-MSN-BTZ.

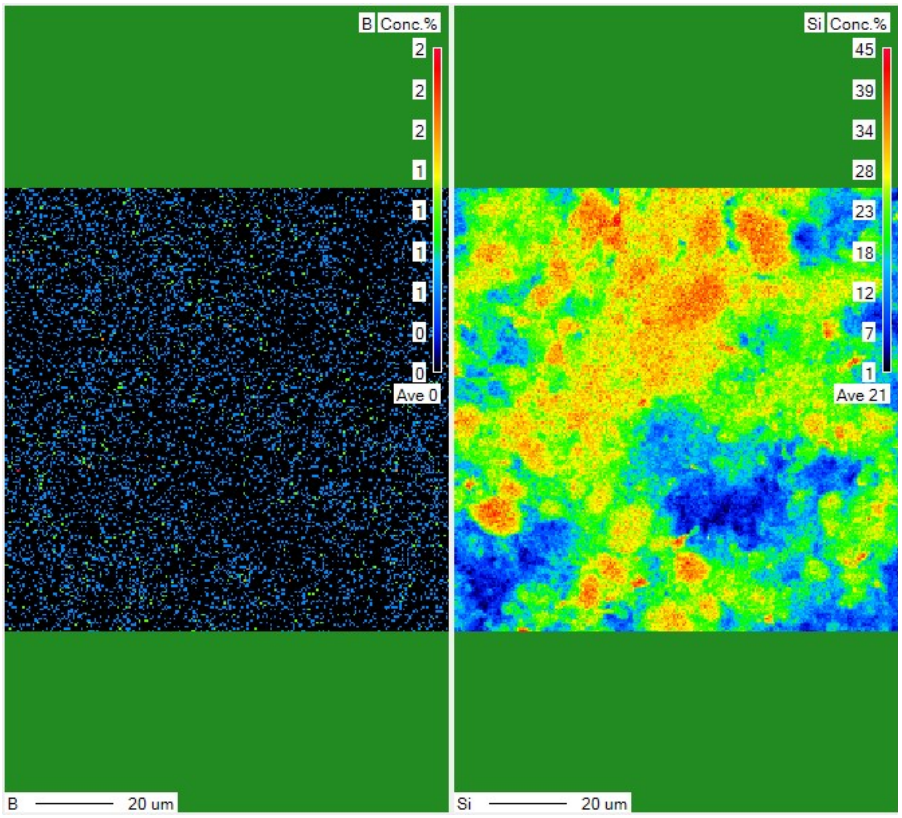

Figure S3. Polychromatic elemental maps for sample MF-MSN-BTZ.

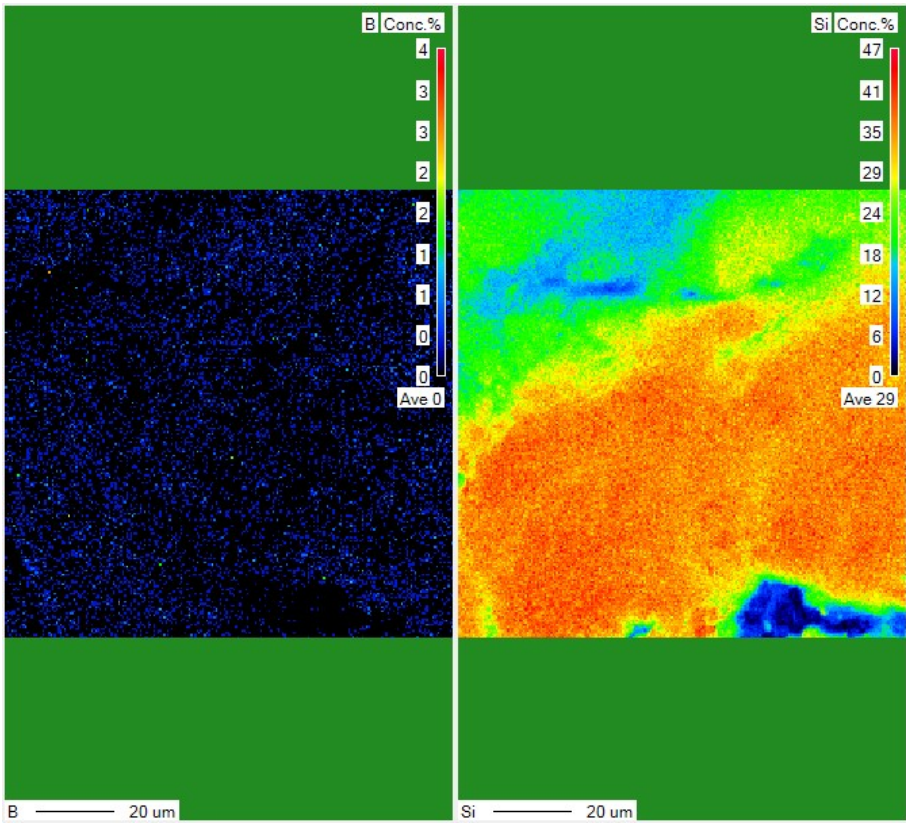

Figure S4. Polychromatic elemental maps for sample HF-MSN-BTZ.

Zeta Potential analysis

Typically, starting MSNs exhibit a negatively charged surface due to the presence of silanol groups, showing a Zeta potential value of approximately – 30 mV. APTES grafting caused an inversion of Zeta potential, from negative to positive values, due to APTES amine moieties.

Several studies reported a greater and more selective uptake of cationic nanoparticles by tumor endothelial cells compared to anionic and neutral nanodevices [11] due to the natural capability to interact with anionic cell membranes, enhancing tumor accumulation efficiency and, so, therapeutic efficacy.[12]

Study of the stability of the HF-MSN-BTZ suspension before the administration

Nanoparticle (NPs) properties such as size, shape, composition, surface chemistry and charge, affect their performance in biological systems. Their capability to target and enter tissues from the blood is greatly related to their behavior in blood flow.[13]

Blood is remarked as a multi-component Non-Newtonian fluid, which is constituted of plasma, red blood cells (RBCs), white blood cells (WBCs), and platelets.[14]

Owing to the complexity of blood flow and its intrinsic properties, particles (platelets, WBCs, RBCs, and NPs) experience different kinds of forces, including Brownian, gravity, thermal buoyancy-induced and external forces. [15, 16]

These forces will influence their motions under specific circumstances. Because of the complexities of microvascular blood flow, the transport and deposition of NPs are expected to be more complicated, and the comprehension of their fate needs more specific and detailed researches. The introduction into the hematic fluid represents a deep change in all the conditions governing the suspendability of the particles. The injection of the suspension is responsible for the fate of the particles and drug in mice organism. To better understand and learn about nanoparticles fate and transport in biological media, fast and screening instruments that can provide key parameters, like stability, are required.

The Turbiscan technology provides suitable information about the potential stability of pharmaceutical formulations and suspensions.[17]

Turbiscan analyzer was employed to assess the experimental stability grading of the FOL-MSN-BTZ and FOL-MSN prototypes, reproducing the *in vivo* administration conditions.

The operating principle of a Turbiscan is based on multiple light scattering techniques. Two detectors, transmission and backscattering, scan the length of the sample acquiring data every 30 s. The stability analysis results from Turbiscan analyzer are measured in Turbiscan Stability Index (TSI) that illustrates how fast the particles contained in the suspension sediment. A lower value of TSI means a more stable sample.

The stability of the suspensions in physiological medium was evaluated for FOL-MSN-BTZ and FOL-MSN (2 mg/kg BTZ EQ) under the same conditions for the in vivo administrations. The data show a linear decrease of stability over time (**Figure S5a**), while maintaining, for each sample, TSI values < 4 in the first 10 minutes (**Figure S5b, S5c, and S5d**), such as to ensure the correct administration of the selected doses.

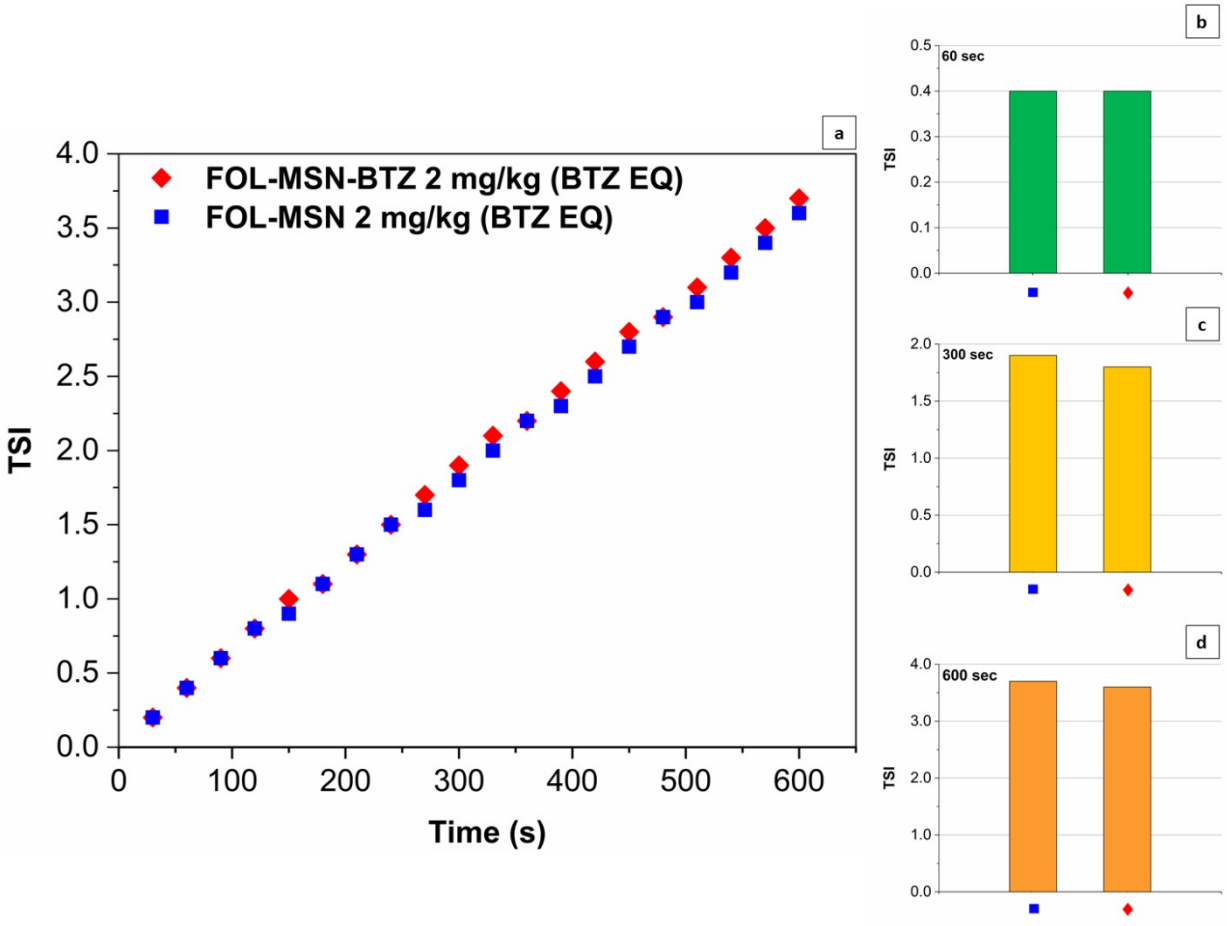

Figure S5. TSI values over time for FOL-MSN-BTZ and FOL-MSN (**a**); comparison of TSI value of the two samples at 60 s (**b**) 300 s (**c**) 600 s (**d**).

Antitumor efficacy

Since the mice were randomized based on tumor volume, all the treatment groups showed comparable tumor volumes at baseline, reported to be 243.678 g (iqr = 141.675-368.541). The mixed-effects models (**Table S2**) showed a significant effect of time (Model 1, coefficient: 0.060, 95%CI 0.048 to 0.073, P<0.001) on tumor

volume that was likely to increase across measurements. In addition, tumor bearing mice treated with FOL-MSN-BTZ were more likely to have a lower tumor volume as compared to untreated animals regardless of value of time in the selected follow-up period (Model 1, coefficient: -1.095, 95%CI -1.668 to -0.523, P<0.001). Considering a model with also a term for the interaction between treatment and time, treatment group effects at baseline were not statistically significant, while time effect showed that in untreated animals tumor volume was likely to increase across measurements (Model 2, coefficient: 0.137, 95%CI 0.121 to 0.154, P<0.001). The statistically significant interaction between time and treatment (P<0.001) indicated that the effect of time depends on treatment received. A potential benefit associated with the FOL-MSN-BTZ treatment was supported by the difference between groups over time as determined from the negative interaction term (Model 2, coefficient -0.156, 95%CI -0.179 to -0.133, P<0.001). Different growth rates (slopes) were shown for BTZ (coefficient -0.087, P<0.001) and FOL-MSN (coefficient -0.036, P=0.002) treatment groups as compared with untreated animals. Contrasts of average marginal effects confirmed that the slope for untreated animals was significantly different from other treatment groups. However, pairwise contrasts at the 5% level endorsed only differences between FOL-MSN-BTZ 2mg/kg (BTZ EQ) treated animals vs. untreated animals and other treatment groups (BTZ 1mg/kg and FOL-MSN-BTZ 2mg/kg BTZ EQ) along with differences between BTZ 1mg/kg treated animals and untreated animals. Evaluating untreated vs. other groups differences for different time points considering conditional marginal effects. Differences were statistically significant from day 7 and day 14 for FOL-MSN-BTZ 2mg/kg BTZ EQ treated animals and BTZ 1mg/kg treatment group, respectively.

	Model 1		**Model 2**	
Effect	**coefficient (95% CI)**	**p-value**	**coefficient (95%CI)**	**p-value**
Time (days)	**0.060 (0.048 to 0.073)**	**<0.001**	**0.137 (0.121 to 0.154)**	**<0.001**
Treatment (reference untreated)				
Tumor+BTZ	**-0.453 (-1.009 to 0.102)**	**0.110**	**0.415 (-0.198 to 1.028)**	**0.185**
Tumor+FOL-MSN	**-0.36 (-0.932 to 0.193)**	**0.198**	**0.013 (-0.600 to 0.627)**	**0.966**
Tumor+FOL-MSN-BTZ	**-1.095 (-1.668 to -0.523)**	**<0.001**	**0.350 (-0.279 to 0.980)**	**0.275**

Interaction **Time X Treatment** Tumor+BTZ Tumor+ FOL-MSN Tumor+FOL-MSN-BTZ	-	-	**-0.087 (-0.110 to -0.064)** **-0.036 (-0.059 to -0.013)** **-0.156 (-0.179 to -0.133)**	**<0.001** **0.002** **<0.001**

Table S2. Mixed-effects model for tumor volume.

Supplementary Figures

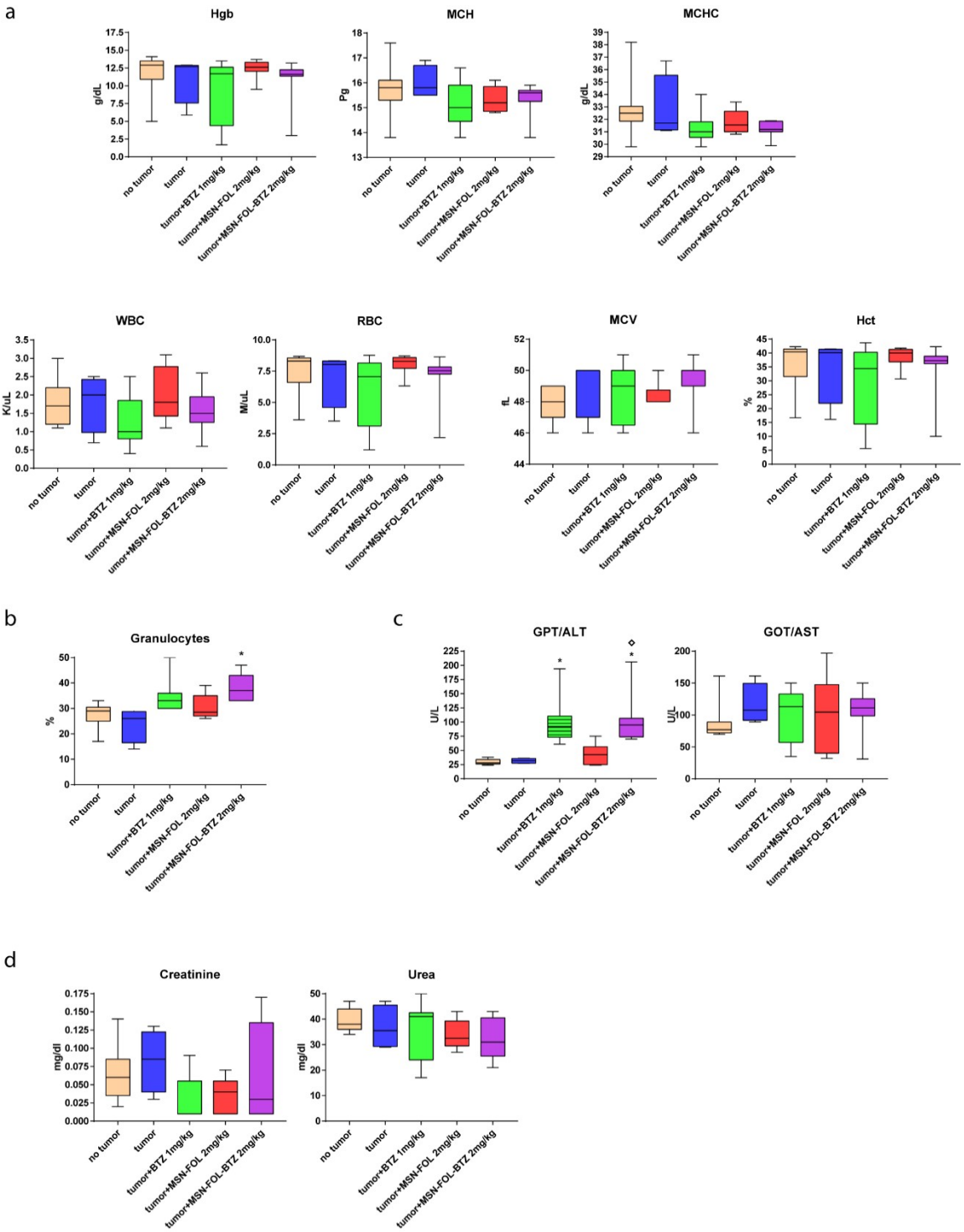

Figure S6. a) Hematology. White blood cells (WBC), red blood cells (RBC), mean corpuscular volume (MCV), hematocrit (HCT), hemoglobin (HGB), mean corpuscular hemoglobin (MCH), mean cell hemoglobin concentration (MCHC), platelets (PLT), mean platelet volume (MPV), plateletcrit (PCT) are reported. **b) Granulocytes. c) Hepatic markers.** ALT= Alanine transaminase or GPT= glutamate-pyruvate transaminase, AST= Aspartate transaminase or GOT= glutamate-oxaloacetate transaminase. **d) Renal markers.** The results were statistically analyzed using the analysis of variance (ANOVA) and the non-parametric Kruskal-Wallis statistic, Graphpad Prism (* $p<0.01$ *vs* tumor; ◊ $p<0.01$ *vs* tumor + FOL-MSN).

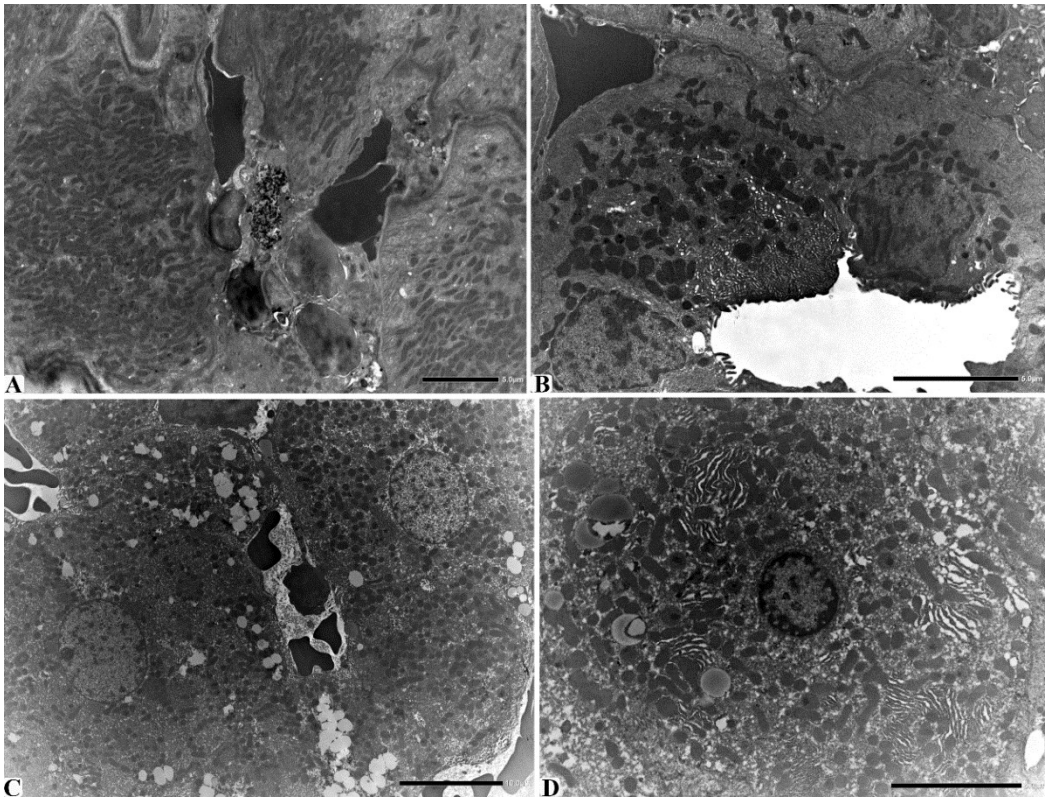

Figure S7. Kidney **(A, B)** and liver **(C, D)** have been explanted, at sacrifice, from FOL-MSN-BTZ animals. TEM micrographs show that both tissues maintain their ultrastructural integrity and general architecture. In the kidney, nanoparticles are seen to flow in the vessel without affecting the organization of renal cell (A). Panel B shows the electrondense (dark) cells of the collecting duct that contain numerous well-organized mitochondria. The apical cytoplasm is tipically highly vacuolated. In the liver, the hepatocytes (C, D) display the canonical organization as single-cell plates separated by vascular channels (sinusoids). Hepatocytes are normally arranged and contains numerous mitochondria and lipid droplets.

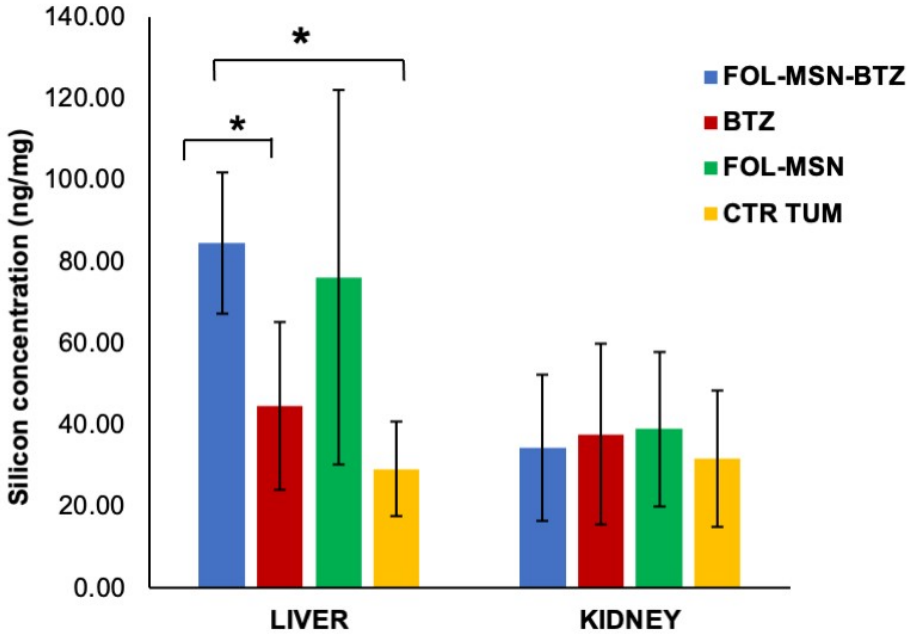

Figure S8. Comparison of silicon amounts in liver and kidney tissues of mice untreated (CTR TUM) and treated with FOL-MSN-BTZ , FOL-MSN, and free BTZ statistically analyzed using the non-parametric Kruskal-Wallis test (* $p<0.05$).

Supplementary Tables

Treatment groups	# mouse	Sacrifice reason	Administrations				
			1	2	3	4	5
Untreated Tumor	6						X
	9	ulcerated tumor			X		
	10						X
	11	tumor volume exceed 10% of body weight			X		
	12	tumor volume exceed 10% of body weight		X			
	13	tumor volume exceed 10% of body weight			X		
	14	ulcerated tumor			X		
	15	tumor volume exceed 10% of body weight		X			
	16	tumor volume exceed 10% of body weight			X		
	17						X
	49	tumor volume exceed 10% of body weight			X		
Tumor + BTZ 1mg/Kg	18						X
	19						X
	20						X
	21						X
	22						X
	23	tumor volume exceed 10% of body weight				X	
	24	ulcerated tumor				X	
	25						X
	26						X
	27	tumor volume exceed 10% of body weight		X			
Tumor + FOL-MSN 2 mg/kg	28						X
	29						X
	30	tumor volume exceed 10% of body weight				X	
	31						X
	32	tumor volume exceed 10% of body weight				X	
	33						X
	34	ulcerated tumor			X		
	35	ulcerated tumor		X			
	36	ulcerated tumor				X	

	37						X
Tumor + FOL-MSN-BTZ 2 mg/kg	**38**						X
	39						X
	40						X
	41	ulcerated tumor				X	
	42						X
	43						X
	44						X
	45						X
	47						X

Table S3. Mice sacrifice during xenograft experiment. All treatments were administered once a week for 5 weeks (5 administrations in total over a period of about one month).

Supplementary References

1. J.G. Croissant, Y. Fatieiev, N.M. Khashab, Degradability and Clearance of Silicon, Organosilica, Silsesquioxane, Silica Mixed Oxide, and Mesoporous Silica Nanoparticles, *Adv. Mat.*, 2017, **29**, 1604634.
2. J.G. Croissant, Y. Fatieiev, A. Almalik, N.M. Khashab, Mesoporous Silica and Organosilica Nanoparticles: Physical Chemistry, Biosafety, Delivery Strategies, and Biomedical Applications, *Adv. Healthc. Mater.*, 2018, **7**, 1700831.
3. B. Frigerio, C. Bizzoni, G. Jansen, C.P. Leamon, G.J. Peters, P.S. Low, L.H. Matherly, M. Figini, Folate receptors and transporters: biological role and diagnostic/therapeutic targets in cancer and other diseases, *J. Exp. Clin. Cancer Res.*, 2019, **1**.
4. J. Shen, Y. Hu, K.S. Putt, S. Singhal, H. Han, D.W. Visscher, L.M. Murphy, P.S. Low, Assessment of folate receptor alpha and beta expression in selection of lung and pancreatic cancer patients for receptor targeted therapies, *Oncotarget,* 2018, **9**, 4485.
5. S. Rijnboutt, G. Jansen, G. Posthuma, J.B. Hynes, J.H. Schornagel, G.J. Strous, Endocytosis of GPI-linked Membrane Folate Receptor-t, *J. Cell Biol.*, 1996, **132**, 35.
6. B. Frigerio, C. Bizzoni, G. Jansen, C. P. Leamon, G. J. Peters, P. S. Low, L. H. Matherly, M. Figini, J. Exp. Clin. Cancer Res., 2019, **38**, 125.
7. V.T.D.M. Hungria, E.D.Q. Crusoé, R.I. Bittencourt, A. Maiolino, R.J.P. Magalhães, J.D. Nascimento Sobrinho, P.Y. Tanaka, New proteasome inhibitors in the treatment of multiple myeloma, *Hematol. Transfus.Cell Ther*., 2019, **41**, 76.
8. J. Adams, V.J. Palombella, E.A Sausville, J. Johnson, A. Destree, D.D. Lazarus, J. Maas, C.S. Pien, S. Prakash, P.J. Elliott, Proteasome inhibitors: a novel class of potent and effective antitumor agents, *Cancer Res*., 1999, **59**, 2615.
9. C.M. Pickart, M.J. Eddins, Ubiquitin: structures, functions, mechanisms, *Biochim. Biophys. Acta, Mol. Cell Res.*, 2004, **1695**, 55.
10. S. A. Bagshaw, E. Prouzet, T. J. Pinnavaia, Templating of mesoporous molecular sieves by nonionic polyethylene oxide surfactants, Science, 1995, **269**, 1242-1244.
11. E. Fröhlich, The role of surface charge in cellular uptake and cytotoxicity of medical nanoparticles, *Int. J. Nanomedicine,* 2012, **7**, 5577.
12. S. Jambhrunkar, Z. Qu, A. Popat, J. Yang, O. Noonan, L. Acauan, Y.A. Nor, C. Yu, S. Karmakar, Effect of Surface Functionality of Silica Nanoparticles on Cellular Uptake and Cytotoxicity, *Mol. Pharm*., 2014, **11**, 3642.
13. M.J. Mitchell, M.M. Billingsley, R.M. Haley, M.E. Wechsler, N.A. Peppas, R. Langer, Engineering precision nanoparticles for drug delivery, *Nat. Rev. Drug Discov.*, 2021, **20**, 101.
14. K. Müller, D.A. Fedosov, G. Gompper, Understanding particle margination in blood flow – A step toward optimized drug delivery systems, *Med. Eng. Phys.*, 2016, **38**, 2.
15. A. Farutin, C. Misbah, Analytical and Numerical Study of Three Main Migration Laws for Vesicles Under Flow, *Phys. Rev. Lett.*, 2013, **110**, 108104.
16. Q.M. Qi, E.S. Shaqfeh, Theory to predict particle migration and margination in the pressure-driven channel flow of blood, *Phys. Rev. Fluids*, 2017, 2, 093102.
17. C. Celia, M. Locatelli, F. Cilurzo, D. Cosco, E. Gentile, D. Scalise, M. Carafa, C.A. Ventura, M. Fleury, C. Tisserand, R.C. Barbacane, M. Fresta, L. Di Marzio, D. Paolino, Long Term Stability Evaluation of Prostacyclin Released from Biomedical Device through Turbiscan Lab Expert, *Med. Chem.*, 2015, **11**, 391.